Numerical Investigation of Fluid Mixing in a Micro-Channel Mixer with Two Rotating Stirrers by Using the Incompressible SPH Method

Shamsoddini, Rahim*[+]

Department of Mechanical Engineering, Sirjan University of technology, Sirjan,, I.R. IRAN

ABSTRACT: *Fluid mixing is a crucial and challenging process for microfluidic systems, which are widely used in biochemical processes. Because of their fast performance, active micromixers that use stirrer blades are considered for biological applications. In the present study, by using a robust and convenient Incompressible Smoothed Particle Hydrodynamics (ISPH) method, miscible mixing within a two-blade micromixer is investigated. The problem discussed herein is represented by an active micromixer comprising two stir-bars that rotate to mix the fluids. Because of its Lagrangian nature, Smoothed Particle Hydrodynamics is an appropriate and convenient method for simulating moving boundary problems and tracking the particles in the mixing process. Previous investigations have been carried out for mixing flow for a low Schmidt number. However, a low Schmidt number is barely applicable for liquid mixing. Hence, in the present study, the Schmidt number is considered to be Sc=1000. The present results show that the two-blade micro-channel mixer considerably improves the mixing rate in comparison with the one-blade micro-channel mixer.*

KEYWORDS: *Micromixer; SPH; Two-stirrer.*

INTRODUCTION

Mixing, as a transport phenomenon, is usually carried out to reduce inhomogeneity in species, temperature, and phases. Fluid mixing is one of the most important phenomena in the chemical and medical industries [1]. Lab-on-a-chip technology has been used in a wide range of processes such as organic synthesis, enzyme assay, protein folding, biological screening, analytical assay, cell analysis, bioprocess optimization, clinical diagnostics, drug delivery studies, nanoparticle crystallization, extraction, and polymerization [2]. These processes are generally implemented with a microscale mixer. Depending on whether an external energy source is applied, micromixers can be classified as passive or active mixers [1–3]. Passive micromixers are completely based on pumping energy. In contrast to passive micromixers, active micromixers use external energy sources to improve mixing. These external energy sources include induced-charge electrokinetic flow ultrasound, acoustic, bubble-induced vibrations, electrokinetic instabilities, the periodic variation of flow rate, the electrowetting-induced merging of droplets, piezoelectric vibrating membranes, magneto-hydrodynamic action, small impellers, and integrated microvalves/pumps, among others [1].

***** *To whom correspondence should be addressed.*
+ E-mail: shamsoddini@sirjantech.ac.ir
1021-9986/2017/5/173-183 11/$/6.10

In the present study, a full Lagrangian approach is applied to investigate a two-stirrer micromixer. Recently, full Lagrangian approaches have been used to model mixing phenomena [4–6]; these methods are based on particle methods. Among particle methods, Smoothed Particle Hydrodynamics (SPH) is one of the first approaches which have been used to simulate mixing phenomena; *Robinson et al.* [5] modeled a twin cam mixer by using SPH. *Shamsoddini et al.* [6] simulated micromixing phenomena within a cylindrical paddle mixer by using a modified SPH scheme.

No modeling is needed for convective terms for SPH modeling; convective terms are satisfied directly by the motion of the particles. Each particle in the mixing flow can also be directly tracked. The SPH method was first proposed for astrophysical applications by *Gingold & Monaghan* [7] and *Lucy* [8]. Since then, it has been extended to model a wide range of engineering applications such as fluid flows and transport phenomena. For SPH, two approaches are generally used to specify the pressure field. The first of these, known as Weakly Compressible SPH (WCSPH), uses an appropriate equation of state to relate pressure variations to density variations. The second, Incompressible SPH (ISPH) solves the Poisson pressure equation to detect the pressure. The SPH is also a suitable method for moving boundary and Fluid-Structure Interaction (FSI) problems because of its Lagrangian nature. It has been widely used to simulate FSI problems [9–12], two-phase flow immiscible [13, 14], and miscible flows [15].

Stir-bar micromixers are applicable in biological laboratory-on-a-chip applications [16]. These have been widely investigated experimentally and numerically; *Lu et al.* [16] presented an active mixer employing micro-magnetic rotating bar stirrers and arrays for microscale fluid mixing in biological laboratory-on-a-chip applications. They found that mixing efficiency can be enhanced by increasing the stirring speed. *Ryu et al.* [17] presented the design and fabrication of a micro stir-bar in surface-micromachined Parylene housings and channels.

This type of active micromixer has also been widely investigated numerically [18–22], with studies examining mixing flow for a low Schmidt number. However, a low Schmidt number is barely applicable for liquid mixing. Hence, in the present study, the Schmidt number is considered to be Sc=1000. For high Schmidt numbers, mass diffusion is very slow in comparison with the advection transport. Therefore, low-velocity flows are more efficient. For micro scales, the viscous effects are dominant. Thus, the chaotic mixing downstream of each stirrer blade is immediately damped. Hence, increasing the number of stirrers could help achieve fast and proper mixing. Although a mixer with two rotating blades has been investigated for circular chambers [23], a mixer with two blades in a channel has not. Therefore, in the present study, the mixing performance of a two-blade micromixer is investigated and the effects of the stirrer size and angular velocity on the mixing rate are discussed.

In the following, the formulation and numerical procedure are first discussed and then the results and discussion are presented.

NUMERICAL PROCEDURE

The SPH formulation is based on an integral form; each continuously defined function f over an interest domain Ω can be expressed as

$$\mathrm{f}(\boldsymbol{r})=\int_{\Omega}\mathrm{f}(\boldsymbol{r})\mathrm{W}(\boldsymbol{r}-\boldsymbol{r}',\mathrm{h})\mathrm{d}\boldsymbol{r}', \tag{1}$$

Where $\boldsymbol{r}$ and $\boldsymbol{r}'$ are respectively the position vector and sub integral variable, W is the kernel function and h is the smoothing length. This equation is approximated by a numerical summation on the discrete points in the domain Ω:

$$\mathrm{f}(\boldsymbol{r})=\sum_{\mathrm{j}}\forall_{\mathrm{j}}\mathrm{f}_{\mathrm{j}}\mathrm{W}(\boldsymbol{r}-\boldsymbol{r}_{\mathrm{j}},\mathrm{h}), \tag{2}$$

Where $\forall_j$ is the volume of the *j*th particle. In the present study, the fifth-order Wendland kernel is used [24]. The use of this kernel function improves the accuracy of fluid flow modeling [25].

$$\mathrm{W}(\mathrm{r},\mathrm{h})=\mathrm{W}_0\times\begin{cases}\left(1-\frac{\mathrm{r}}{\mathrm{h}}\right)^4\left(4\frac{\mathrm{r}}{\mathrm{h}}+1\right) & 0\le\frac{\mathrm{r}}{\mathrm{h}}<1\\ 0 & \frac{\mathrm{r}}{\mathrm{h}}\ge 1\end{cases}, \tag{3}$$

Where W_0 is $7/\pi h^2$ for two-dimensional cases.

The gradient, divergence, and Laplacian operator for an arbitrary scalar function f or tensor function F are, respectively:

$$\langle \nabla f \rangle_i = \sum_j \forall_j \left(f_j - f_i \right) \boldsymbol{B}_i . \nabla W_{ij}, \tag{4}$$

$$\langle \nabla . \boldsymbol{F} \rangle_i = \sum_j \forall_j \left(\boldsymbol{F}_j - \boldsymbol{F}_i \right) . \left(\boldsymbol{B}_i . \nabla W_{ij} \right), \tag{5}$$

$$\langle \nabla^2 f \rangle_i = \sum_j 2 \forall_j \frac{f_i - f_j}{r_{ij}} \boldsymbol{e}_{ij} . \left(\boldsymbol{B}_i . \nabla W_{ij} \right), \tag{6}$$

$$\langle \nabla^2 f \rangle_i = \hat{\boldsymbol{B}}_{\boldsymbol{i}} : \sum_j 2 \forall_j \boldsymbol{e}_{ij} \nabla W_{ij} \left(\frac{f_j - f_i}{r_{ij}} - \boldsymbol{e}_{ij} . \langle \nabla f \rangle_i \right), \tag{7}$$

Where e_{ij} is the unit vector in the inter-particle direction (from j to i) and B is a corrective tensor for kernel gradients, which has been applied before and examined by *Bonet and Lok* [26]:

$$\boldsymbol{B}_i = - \left[\sum_j \forall_j \boldsymbol{r}_{ij} \nabla W_{ij} \right]^{-1}, \tag{8}$$

and $\hat{\boldsymbol{B}}_{\boldsymbol{i}}$ is a renormalization tensor as offered by *Fatehi and Manzari* [27], which is calculated by using the following set of equations:

$$\hat{\boldsymbol{B}}_{\boldsymbol{i}} : \left[\sum_j \forall_j \boldsymbol{r}_{ij} \boldsymbol{e}_{ij} \boldsymbol{e}_{ij} \nabla W_{ij} + \left(\sum_j \forall_j \boldsymbol{e}_{ij} \boldsymbol{e}_{ij} \nabla W_{ij} \right) \times \boldsymbol{B}_i . \left(\sum_j \forall_j \boldsymbol{r}_{ij} \boldsymbol{r}_{ij} \nabla W_{ij} \right) \right] = -\boldsymbol{I} \tag{9}$$

Eq. (7) is introduced and applied by *Fatehi and Manzari* [27]. In the present study, both Eq. (6) and Eq. (7) are used: Eq. (6) for the pressure Laplacian discretization and Eq. (7) for the diffusion terms in the transport equations.

The governing equations are respectively the mass, momentum, and concentration transport equations:

$$\nabla . V = 0, \tag{10}$$

$$\frac{d\boldsymbol{V}}{dt} = \nabla . \left(\nu \left(\nabla \boldsymbol{V} \right) \right) + \boldsymbol{g} - \frac{\nabla p}{\rho}, \tag{11}$$

$$\frac{dC}{dt} = \alpha \nabla^2 C \tag{12}$$

Where ρ ν, V, p α, and C are respectively the fluid's density, viscosity, velocity, pressure, mass diffusivity, and concentration.

The SPH discretization of the momentum equation will be

$$\frac{\boldsymbol{V}_i^{n+1} - \boldsymbol{V}_i^n}{\Delta t} = \left(\boldsymbol{g} + \langle \nabla . \left(\nu \nabla \boldsymbol{V} \right) \rangle_i - \left\langle \frac{\nabla p^n}{\rho} \right\rangle_i \right). \tag{13}$$

Hence, the velocity can be defined as

$$\boldsymbol{V}_i^{n+1} = \boldsymbol{V}_i^{*,n+1} - \Delta t \left\langle \frac{\nabla p^{n+1}}{\rho} \right\rangle_i, \tag{14}$$

Where $\boldsymbol{V}_i^{*,n+1}$ is the intermediate velocity due to the buoyancy and viscous terms of the fluid particle acceleration:

$$\boldsymbol{V}_i^{*,n+1} = \boldsymbol{V}_i^n + \left(\boldsymbol{g} + \hat{\boldsymbol{B}}_{\boldsymbol{i}} : \sum_j 2 \forall_j \boldsymbol{e}_{ij} \nabla W_{ij} \left(\nu_{ij} \frac{\boldsymbol{V}_j^n - \boldsymbol{V}_i^n}{r_{ij}} - \boldsymbol{e}_{ij} . \left\langle \nu_{ij} \nabla \boldsymbol{V} \right\rangle_i^n \right) \right) \Delta t \tag{15}$$

For the incompressible flow (using Eq. (10)), applying the divergence operator in Eq. (14) leads to the pressure Poisson equation:

$$\nabla . \left(\frac{1}{\rho} \nabla p^{n+1} \right)_i = \frac{\nabla . \boldsymbol{V}_i^{*,n+1}}{\Delta t} \tag{16}$$

To solve the above equation, another system of equations is needed. This is solved explicitly by using a method similar to the Gauss-Seidel method; the iterative SPH discretization of the above equation will be

$$\left(P_i^{n+1} \right)^{k+1} = \left(\frac{\left(\sum_j 2 \frac{\forall_j}{\rho} \frac{p_j^{n+1}}{r_{ij}} \boldsymbol{e}_{ij} . \left(\boldsymbol{B}_i . \nabla W_{ij} \right) + \frac{1}{\Delta t} \sum_j \forall_j \left(\boldsymbol{V}_j^{*,n+1} - \boldsymbol{V}_i^{*,n+1} \right) . \left(\boldsymbol{B}_i . \nabla W_{ij} \right) \right)}{\sum_j 2 \frac{\forall_j}{\rho r_{ij}} \boldsymbol{e}_{ij} . \left(\boldsymbol{B}_i . \nabla W_{ij} \right)} \right)^k \tag{17}$$

Where k is the iteration number. The iteration is continued until the variations P_i^{n+1} become very small.

In the corrector step, the velocity is corrected by using the pressure force acceleration:

$$\boldsymbol{V}_i^{n+1} = \boldsymbol{V}_i^{*,n+1} - \left\langle \frac{\nabla p}{\rho} \right\rangle_i^{n+1} \Delta t. \tag{18}$$

Finally, the particle position is rearranged by

$$\boldsymbol{r}_i^{n+1} = \boldsymbol{r}_i^{n} + \boldsymbol{V}_i^{n+1}\Delta t. \quad (19)$$

After the fluid flow determination, the mass transport equation (concentration) is solved as follows:

$$C_i^{n+1} = C_i^{n} + \left(\widehat{\boldsymbol{B}}_{\boldsymbol{i}} : \sum_j 2\alpha \forall_j e_{ij} \nabla W_{ij} \left(\frac{C_j^n - C_i^n}{r_{ij}} - e_{ij}.\langle \nabla C \rangle_i^n \right)\right)\Delta t \quad (20)$$

The boundary conditions that dominate the wall boundaries are the no-slip condition for the velocity and the Neumann boundary conditions for the pressure and mass diffusion. Two layers of dummy particles are arranged close to each wall boundary, similar to those particles defined by *Lee et al.* [28]. These particles have the same velocity as their corresponding wall particles. The dummy particles also have the same pressure and concentration as the wall in the normal direction to satisfy the Neumann boundary condition.

For the moving boundary condition, the pressure boundary condition is achieved as follows:

$$\left(\frac{\nabla p}{\rho}\right).n_w = -a.n_w + \nu \nabla^2 V.n_w + g.n_w \quad (21)$$

Where a is the acceleration and n_w is the normal vector of the surface. If the body is fixed or moves with constant velocity or the normal vector of the surface is perpendicular to the acceleration vector (such as narrow blade rotation with constant angular velocity), this equation is simplified to the following form:

$$\left(\frac{\partial p}{\partial n_w}\right) = 0 \quad (22)$$

The periodic boundary condition is defined for the flow boundaries. For the periodic boundary condition, each particle that exits the outlet is copied at the same position in the section at the inlet. To create a fluid flow in the channel, the body acceleration g_x can be imposed on the fluid particles. This axial acceleration generates a flow that is the same as the case when $\Delta p = \rho g_x L$ is applied on the ends of the channels [12]. For the present periodic boundary condition, particles' velocities are renormalized to the parabolic velocity profile for the inlet sections, in line with *Sefid et al.* [12]. Because of the presence of the bluff body, the particle velocity is renormalized according to the parabolic velocity profile:

$$u_i = \frac{3}{2} U_{ave} \left(1 - \left(\frac{y_i}{H/2}\right)^2\right) \quad (23)$$

Where y_i is the distance from the center line, H is the channel width, and U_{ave} is the average velocity. The average velocity for this renormalization is calculated by averaging the particles' velocities at the outlet section. To calculate U_{ave}, the summation of the velocity of all the particles between L-h and L is divided by the number of these particles.

Defects, tensile instability, and particle clustering are complications and unfavorable phenomena in the SPH simulations. To avoid these, a shifting algorithm – similar to the particle shifting approach of *Xu et al.* [29] – is defined in the present study. The direction and amount of shifting are determined from the arrangement of neighboring particles, with Δr defined as the shifting particle vector calculated by

$$\Delta r_i = \varepsilon \bar{r}_i \quad (24)$$

Where ε can vary between 0 and 0.1 and $\bar{r}_i$ is equal to

$$\bar{r}_i = \sum_j \forall_j r_{ij} W_{ij} \quad (25)$$

If the particles are homogeneously distributed around particle i, then $\bar{r}_i$ will be zero. Otherwise, this vector shows that the distribution of neighboring particles around particle i is not balanced. Then, the particle is slightly shifted by Δr. Ultimately, it is necessary to modify the flow field variables in the new position. According to the first-order Taylor series expansion, these modifications are

$$\Delta V_i = \Delta r_i.\langle \nabla V \rangle_i \quad (26)$$

$$\Delta p_i = \rho_i \Delta r_i.\left\langle \frac{\nabla p}{\rho} \right\rangle_i \quad (27)$$

$$\Delta C_i = \Delta r_i.\langle \nabla C \rangle_i \quad (28)$$

For the present algorithm, the time step ($\Delta t = t^{n+1} - t^n$) is calculated from the equation:

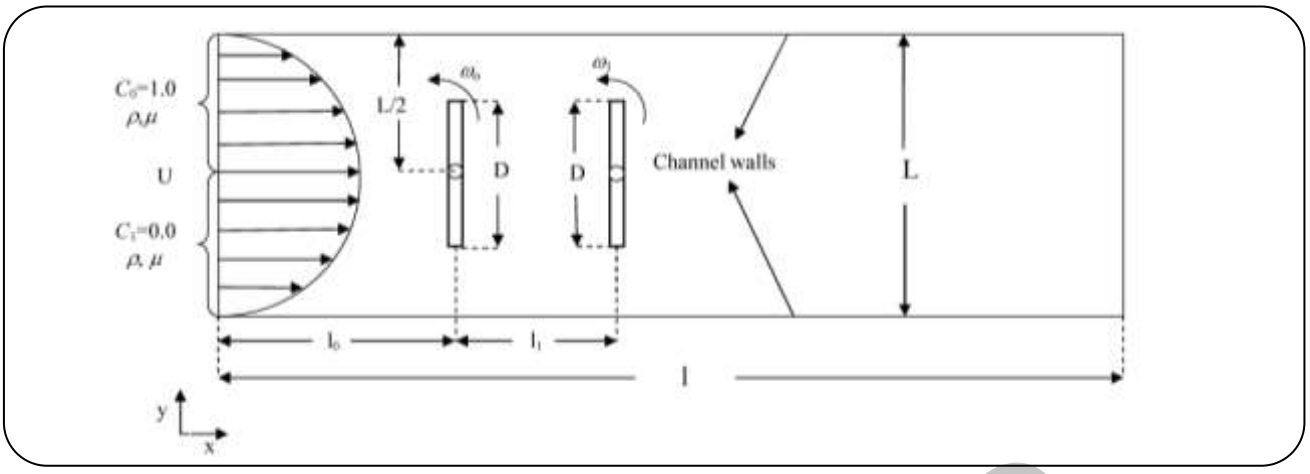

Fig. 1: Scheme of the two-stirrer micromixer.

$$d\Delta t = \beta_t \min\left(\frac{\delta_{min}}{V_{max}}, \frac{\delta_{min}^2}{\upsilon}, \sqrt{\frac{\delta_{min}}{g}}, \frac{\delta_{min}^2}{\alpha}\right) \quad (29)$$

Where β_t is a constant coefficient that can be between 0 and 1, δ_{min} is the minimum distance between two neighboring particles, and V_{max} is the maximum velocity of the particles. All numerical simulations were performed on an Intel System Core i5- 3450 CPU @ 3.10 GHz (4 GB RAM).

RESULTS AND DISCUSSION

The problem discussed herein is represented by an active micromixer comprising two stir-bars that rotate to mix the fluids. The scheme of the micromixer is shown in Fig. 1.

Some experimentally observed mixing phenomena can be produced by using 2D modeling in the microchannel mixer [30, 31]. Hence, a two-dimensional model is considered for the present simulations. The length of the channel, stir-bar, distance between the inlet and position of the first stirrer, distance between the stirrers, and width of the channel are specified by l, D, l_0, l_1, and L, respectively, where L=0.00075 m and l=10 L. The inlet fluids have the same density and viscosity but different concentrations, termed C_0 and C_1. The blades can rotate in the same or opposite directions. For the present study, a high Schmidt number (Sc=1000) is considered and the effects of the stirrer frequency and size on the mixing flow for a two-stirrer micromixer are investigated. For the SPH simulations, the solution parameters are h=2.7δ (where δ is the initial particle space), $\varepsilon = 0.1$, and β_t=0.5.

One of the major complications of the present simulations is arranging the dummy particles for the blade regions. The smoothing length and number of dummy rows are adjusted precisely; the dummy particles defined for one side of the blade cannot be placed in the kernel radius of the particles on the other side of the blade. In the present simulation, two rows of dummy particles are considered for each wall boundary. To investigate the mixing behavior, a dimensional analysis is performed and the obtained non-dimensional groups are shown in Table 1. In this table, Π_1 to Π_4 are geometrical non-dimensional groups. Except $\phi o \rho$ Π_1, the geometrical non-dimensional groups are assumed to be constant. N is the number of stirrer blades and n is the number of rotation cycles.

Before applying the present code to a typical problem, it is validated by using a similar study. To validate the present algorithm, the mixing fluid due to the vertical oscillation of a confined circular cylinder in a channel is examined. The scheme of the problem involving geometry and dimensions is shown in Fig. 2. This problem has been solved by *Celik and Beskok* [32]. Hence, the results of the present algorithm are validated by their results for the case $Sc=Pe_D/Re_D=1.0$, $Re_D=100$, and $f_f/f_0=1.0$, where f_0 is the natural frequency of the vortex shedding and f_f is the forced frequency of the cylinder oscillation.

The result of the present simulation for the mixing index in comparison with *Celik and Beskok's* [32] results is shown in Fig. 3. The mixing index is defined as follows:

Table 1: Non-dimensional groups for the investigation of a two-stirrer micromixer.

number	Non- dimensional Groups	Value
Π_1	L/D	variable
Π_2	l / L	10
Π_3	l_0 /L	2
Π_4	l_1 /L	1.975
Π_5	$D\omega_0/U$	variable
Π_6	Re=(UL/v)	variable
Π_7	Sc=(v/α)	1000
Π_8	D_t	variable
Π_9	n	variable
Π_{10}	N	variable

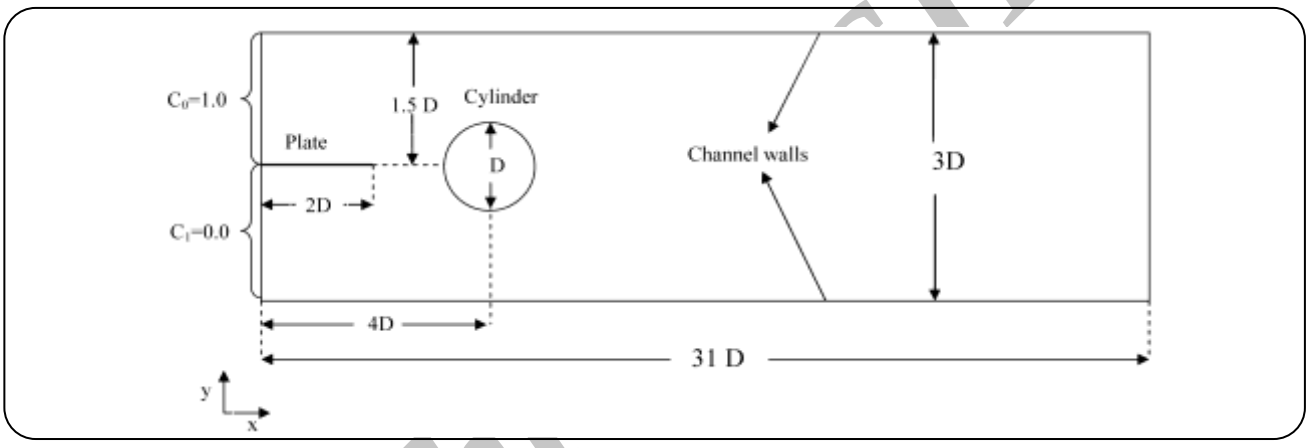

Fig. 2: Scheme and dimensions considered for the investigation of fluid mixing due to the vertical oscillation of a confined circular cylinder in a channel.

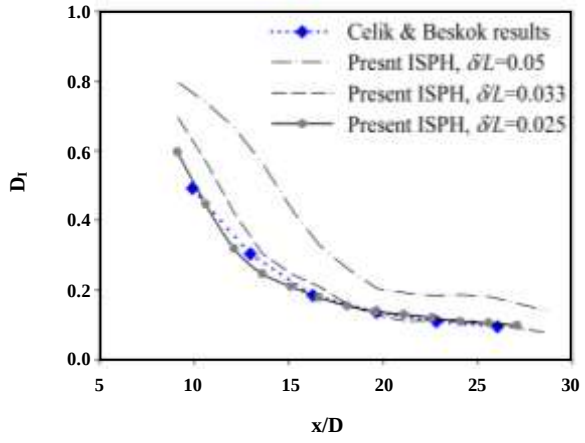

Fig. 3: Variations in the mixing index along the channel for the present simulation in comparison with Celik and Beskok's [32] results.

$$D_I = \sqrt{\frac{1}{N_p}\sum_{i=1}^{N_p}\left(\frac{C_i - C_{mean}}{C_{mean}}\right)^2} \qquad (30)$$

Where N_p is the number of sample particles in a cross-section of the channel, C_{mean} is the mean concentration at the inlet, and C_i is the local concentration in the same section indicated by the concentration of the *i*-th particle. In Figure 3, the effect of the particle space on accuracy is also shown; as the particle space decreases (i.e. an increasing particle number), accuracy increases. The results show that δ/L=0.025 is an adequate and accurate particle space for the SPH calculation of the present simulations. The contour concentration, vorticity, and pressure distribution are shown in Fig. 4.

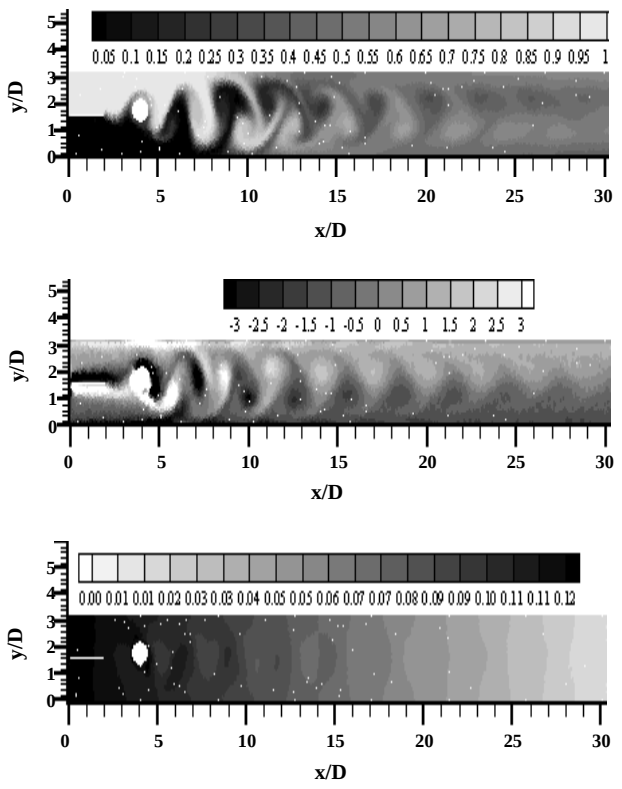

Fig. 4: Contours of the concentration (A), vorticity (B), and (C) pressure distribution for the present SPH simulation.

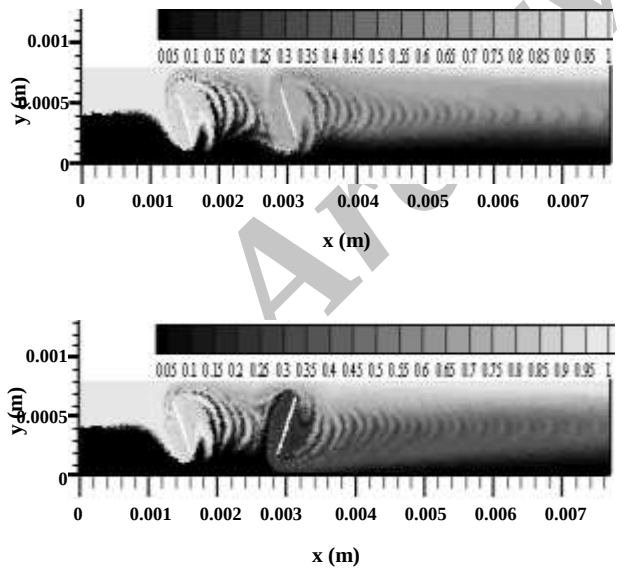

Fig. 5: Contours of the concentration distribution for the case of L/D=1.6, Re=1.25, $D\omega_0/U$=15.8, for two distinct rotation situations, ω_0/ω_1=1 and ω_0/ω_1=–1.

The standard SPH method (WCSPH) suffers from non-physical fluctuations, especially in the pressure field [28]. However, the ISPH method applied in the present study can properly remove these non-physical fluctuations. As shown in Fig. 4C, the pressure field is smooth and there are no non-physical fluctuations.

As shown in Fig. 4, for a high Reynolds number and low Schmidt number, vortex shedding plays an important role in increasing the mixing rate. However, vortex shedding may be ineffective with high Schmidt numbers. For micromixers, low Reynolds numbers are more applicable, especially for high Schmidt numbers. However, as mentioned before, previous numerical studies have been carried out for a low Schmidt number [18–22]. In the present study, therefore, the flow and mixing behaviors for a high Schmidt number are considered and discussed.

For the first investigation, the mixing flow for the case of L/D=1.6, Re=1.25, $D\omega_0/U$=15.8, for two distinct rotation situations, ω_0/ω_1 = 1 and ω_0/ω_1 = -1, is considered and investigated. The contours of the concentration distribution for these cases are shown in Fig. 5.

As indicated in Fig. 5, near the blade sweep region (especially the second blade), there is a well-mixed fluid. Mixing strongly occurs in the regions where the bands are formed and stretched. However, the region of well-mixed fluid does not expand further vertically outside the blade sweep region; the particles outside the blade sweep region remain largely unmixed.

Usually, the mixing pattern has a significant effect on the performance of mixers [33]. In Fig. 6, the mainstream and the streams created around the blades are shown separately. While the stirrer rotates, a part of the fluid is engaged with the stirrer and the remaining flow is forced to move downward. For the remaining flow, this process is repeated; a part of the fluid is engaged with the second blade stirrer and the remaining flow is forced to the down or up of the wall of the channel, according to the direction of the rotation of the blade. When the second stirrer rotates in the opposite direction of the first blade, a part of the unmixed region is shifted toward the other wall of the channel. This division in the flow increases the contact area between the unmixed and well-mixed regions. Hence, the mixing rate increases for the case of ω_0/ω_1 = 1 in comparison with the case of ω_0/ω_1 =1.

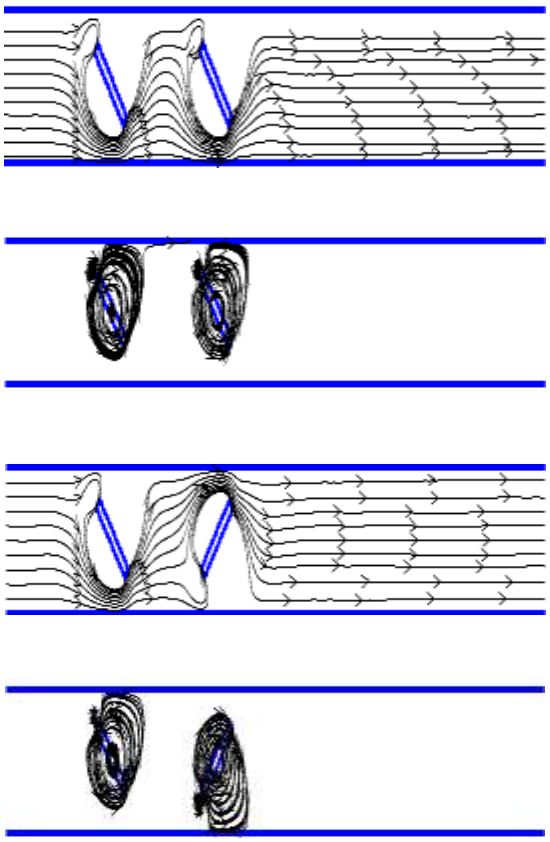

Fig. 6: Stream lines for the case of $\omega_0/\omega_1=1$ (two upper figures) and case of $\omega_0/\omega_1=-1$ (two lower figures).

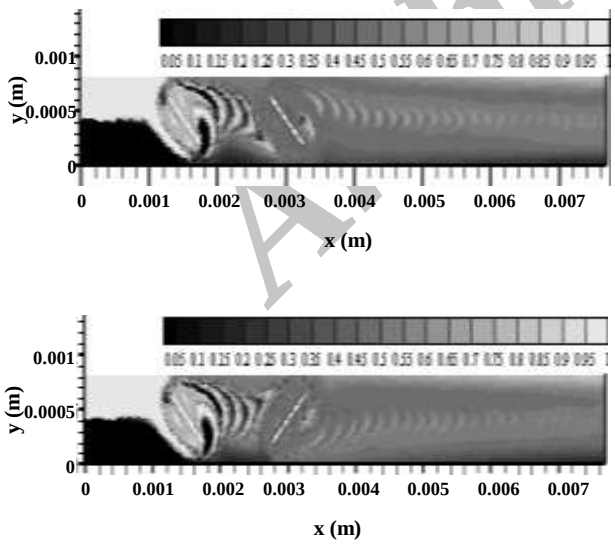

Fig. 7: Contours of the concentration for the case of Re=1.25, L/D=1.176, $D\omega_0/U$=15.8 and $\omega_0/\omega_1=1$ (upper figure) and $\omega_0/\omega_1=-1$ (lower figure).

Those parts of the fluid engaged with the stirrer blades separate gradually. The blade rotation creates regular bands in the flow field. These crescent-shaped bands increase the contact area between the fluids. Basically, fluid mixing is a process that involves the reduction of length scales by stretching and folding the material lines or surfaces [34]. Compression, expansion, and blade motions lead to stretching and folding the fluid streams, which helps enhance the mixing rate.

The unmixed regions are observed near the channel walls along the channel. It seems that the stirrer length should be increased to create full channel-width mixing. Hence, L/D decreases to L/D=1.176, while the other non-dimensional groups remain unchanged. Fig. 7 shows the concentration distributions in the channel with two stirrer blades for the case of Re=1.25, L/D=1.176, $D\omega_0/U$=15.8 for both the same direction rotation ($\omega_0/\omega_1 = 1$) and opposite direction rotation ($\omega_0/\omega_1 = 1$). As shown, the unmixed regions for the new cases (L/D=1.176) have become thinner than those for the previous cases (L/D=1.6), and proper mixing ($D_I < 0.2$) occurs at the outlet section.

In Table 2, the results of the present study of the mixing index for the 18 different cases is shown. The results show that the mixing index of the cases with N=2, in comparison with N=1, decreases considerably. It is also indicated that the cases with the same rotation direction ($\omega_0/\omega_1=1$) are as efficient as those with the opposite direction rotation ($\omega_0/\omega_1=-1$) for the case of L/D=1.176. The results also confirm that proper mixing ($D_I < 0.2$) only occurs in the case with two stirrer blades and $D\omega_0/U>11.95$.

The investigations show that increasing the angular velocity leads to faster mixing. However, increasing the angular velocity of the blades for the micro scales is limited [1]. The results also indicate that increasing the angular velocity by more than a certain value does not lead to a higher mixing rate. Fig. 8 shows the variation in the mixing index compared with the number of rotations of the blade (cycle), for the different cases according to the rotation speed. As shown in this figure, increasing the non-dimensional parameter $D\omega_0/U$ from 15.8 to 21 not only does not lead to mixing improvement but also decreases mixing for the same direction rotation case ($\omega_0/\omega_1=1$). It can be concluded that there are limitations when increasing the angular velocity of the blades to improve mixing.

Table 2: Mixing index at the outlet section for the 18 different cases for Re=1.25 and Sc=1000.

case	N	L/D	ω_0/ω_1	$D\omega_0/U$	D_I
1	1	1.176	-	3.98	0.738
2	1	1.176	-	7.96	0.536
3	1	1.176	-	11.95	0.379
4	1	1.176	-	15.8	0.26
5	2	1.6	+1	11.95	0.623
6	2	1.6	–1	11.95	0.611
7	2	1.6	+1	15.8	0.613
8	2	1.6	–1	15.8	0.524
9	2	1.176	+1	3.98	0.549
10	2	1.176	–1	3.98	0.555
11	2	1.176	+1	7.96	0.45
12	2	1.176	–1	7.96	0.515
13	2	1.176	+1	11.95	0.228
14	2	1.176	–1	11.95	0.219
15	2	1.176	+1	15.8	0.156
16	2	1.176	–1	15.8	0.168
17	2	1.176	+1	21	0.162
18	2	1.176	–1	21	0.152

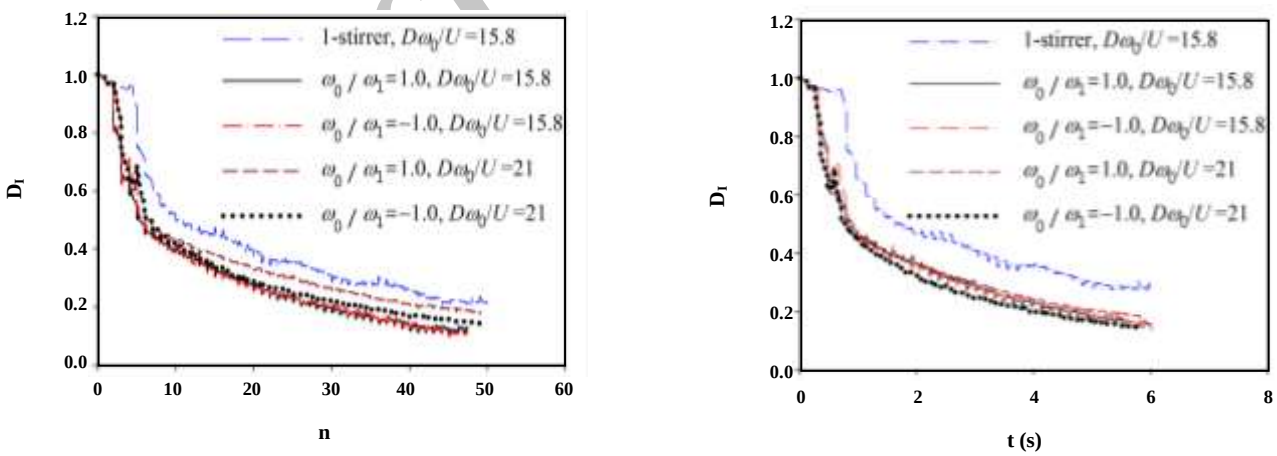

Fig. 8: Variations in the mixing index with the number of rotations of the blades (top) and time (bottom) for cases #4 & #15 to #18 in Table 2.

CONCLUSIONS

In the present study, by using a robust SPH method, mixing flow in a micro-channel equipped with two stirrer blades was investigated. The blades could rotate in the same or in the opposite direction. A dimensional analysis was performed and non-dimensional groups were derived. Eighteen different cases simulated numerically were investigated. The main results are as follows.

The mixing rate depends on the length and number of blades. By increasing the blade length from L/D=1.6 to L/D=1.176, the mixing index decreases by more than 45%. The results also show that the rotation of the blades in the opposite direction of each other ($\omega_0/\omega_1=-1$) improves the mixing rate, especially for smaller blades. The mixing rate is boosted by increasing the angular velocity of the blades. In the same conditions, the two-blade micromixer improves the mixing rate considerably in comparison with the one-blade micromixer (by at least 38%). Among the 18 cases examined, proper mixing only occurs for four cases: N=2, Re=1.25, Sc=1000, L/D=1.176, and $D\omega_0U$>11.95 (case #15 to case #18). It is also concluded that there is a limitation when increasing the angular velocity of the blades to improve mixing.

Received: Mar. 18, 2015 ; Accepted: Jul. 17, 2017

REFERENCES

[1] Nguyen N.T., "Micromixers, Fundamentals, Design and Fabrication", William Andrew Inc., Singapore (2008).

[2] Capretto L., Cheng W., Hill M., Zhang X., Micromixing within Microfluidic Devices, *Top. Curr. Chem*., **304**: 27–68 (2011).

[3] Cook K.J., Fan Y.F., Hassan I., Mixing Evaluation of a Passive Scaled-up Serpentine Micromixer with Slanted Grooves, *ASME J. Fluids Eng*., **135** (8): 081102- 081113 (2013).

[4] Lenaerts T., Dutré P., Mixing Fluids and Granular Materials, *Comput. Graph. Forum*, **28** (2): 213-218 (2009).

[5] Robinson M., Cleary P., Monaghan J., Analysis of Mixing in a Twin Cam Mixer using Smoothed Particle Hydrodynamics, *AIChE Journal*, **54**(8): 1987-1998 (2008).

[6] Shamsoddini R., Sefid M., Fatehi R., Lagrangian Simulation and Analysis of the Micromixing Phenomena in a Cylindrical Paddle Mixer Using a Modified Weakly Compressible Smoothed Particle Hydrodynamics Method, *Asia-Pac. J. Chem. Eng.*, **10**(1): 112-124 (2015).

[7] Gingold R.A., Monaghan J., Smoothed Particle Hydrodynamics: Theory and Application to Non-spherical Stars, *Mon. Not. Roy. Astron. Soc.*, **181**: 375-389 (1977).

[8] Lucy, L.B., A Numerical Approach to the Testing of the Fission Hypothesis, *Astron. J.*, **82**: 1013-1024 (1997).

[9] Rafiee A., Thiagarajan K.P., An SPH Projection Method for Simulating Sluid-Hypoelastic Structure Interaction, *Comput. Methods Appl. Mech. Engrg*., **198**(33-36): 2785–2795 (2009).

[11] Hashemi M.R., Fatehi R., Manzari M.T., A Modified SPH Method for Simulating Motion of Rigid Bodies in Newtonian Fluid Flows, *Int. J. Nonlinear Mech*. **47** (6): 626-638. (2012).

[12] Sefid M., Fatehi R., Shamsoddini R., A Modified Smoothed Particle Hydrodynamics Scheme to Model the Stationary and Moving Boundary problems for Newtonian Fluid Flows, *ASME J. Fluids Eng.*, **137**(3): 031201-9 (2015).

[13] Shadloo M.S., Yildiz M., Numerical Modeling of Kelvin–Helmholtz Instability Using Smoothed Particle Hydrodynamics, *nt. J. Numer. Meth. Eng*., **87** (10): 988-1006 (2011).

[14] Shadloo M.S., Zainali A., Yildiz M., Simulation of Single Mode Rayleigh–Taylor Instability by SPH Method, *Comput. Mech*., **51** (5): 699-715 (2013).

[15] Tartakovsky A.M., Meakin P.A., Smoothed Particle Hydrodynamics Model for Miscible Flow in Three-Dimensional Fractures and the Two-Dimensional Rayleigh–Taylor Instability, *J. Comput. Phys*., **207** (2), 610–620 (2005).

[16] Lu L., Ryu K.S., Liu C., A Magnetic Microstirrer and Array for Microfluidic Mixing, *J. Microelectromech. Syst.*, **11** (5): 462-469 (2012).

[17] Ryu K.S., Shaikh K., Goluch E., Fan Z., Liu C., Micro Magnetic Stir-bar Mixer Integrated with Parylene Microfluidic Channels, *Lab chip* **4** (6): 608-613 (2004).

[18] An S.J., Kim Y.D., Heu S., Maeng J.S., Numerical Study of the Mixing Characteristics for Rotating and Oscillating Stirrers in a Microchannel, *J. Korean. Phys. Soc*., **49** (2): 651-659 (2006).

[19] Kim Y.D., An S.J., Maeng J.S., Numerical Analysis of the Fluid Mixing Behaviors in a Microchannel with a Circular Cylinder and an Oscillating Stirrer, *J. Korean. Phys. Soc.*, **50** (2): 505-513 (2007).

[20] Park J.Y., Kim Y.D., Kim S.R., Han S.Y., Maeng J.S., Robust Design of an Active Micromixer Based on the Taguchi Method, *Sensor Actuat. B*, **129** (2): 790–798 (2008).

[21] Ryu S.P., Park J.Y., Han S.Y., Optimum Design of an Active Micro-mixer Using Successive Kriging Method, *Int. J. Precis. Eng. Manuf.* **12** (5): 849-855 (2011).

[22] Shamsoddini R., Sefid M., Fatehi R., ISPH Modelling and Analysis of Fluid Mixing in a Microchannel with an Oscillating or a Rotating Stirrer, *Eng. Appl. Comp. Fluid Mech.*, **8** (2): 289-298 (2014).

[23] Shamsoddini R., Sefid M., Fatehi R., Numerical Investigation of the Mixing Performance of Two-Blade Twin and Circular Mixers by Using an Improved Weakly Compressible Smoothed Particle Hydrodynamics, *Moderes Mech. Eng.*, **14**(11), 97-105 (1393).

[24] Wendland H., Piecewise polynomial, Positive Definite and Compactly Supported Radial Functions of Minimal Degree, *Adv. Comput. Math*. **4**: 389-396 (1995).

[25] Dehnen W., Aly H., Improving Convergence in Smoothed Particle Hydrodynamics Simulations without Pairing Instability, *Mon. Not. Roy. Astron. Soc*., **425**: 1068-1082 (2012).

[26] Bonet J., Lok T.S., Variational and Momentum Preservation Aspects of Smooth Particle Hydrodynamic Formulation, *Comput. Meth. Appl. Mech. Eng*., **180** (1-2): 97-115 (1999).

[27] Fatehi R., Manzari M.T., Error Estimation in Smoothed Particle Hydrodynamics and a New Scheme for Second Derivatives, *Comput. Math. Appl*. **61** (2), pp. 482-498 (2011).

[28] Lee E.S., Moulinec C., Xu R., Laurence D., Stansby P., Comparisons of Weakly Compressible and Truly Incompressible Algorithms for the SPH Mesh Free Particle Method, *J. Comput. Phys*. **227** (18): 8417–843 (2008) .

[29] Xu R., Stansby P., Laurence D., Accuracy and Stability in Incompressible SPH (ISPH) Based on the Projection Method and a New Approach, *J. Comput. Phys*. **228** (18): 6703–6725 (2009).

[30] Gobby D., Angeli P., Garvriilidis A., Mixing Characteristics of T-type Microfluidic Mixers, *J. Micromech. Microeng*. **11**, 126-132 (2001).

[31] Erickson D., Li D., Microchannel Flow with Patch-wise and Periodic Surface Heterogeneity, *Langmuir* **18**: 8949-8959 (2002).

[32] Celik B., Beskok A., Mixing Induced by a Transversely Oscillating Circular Cylinder in a Straight Channel, *Phys. Fluids*, **21**: 073601 1-9 (2009).

[33] Gorji M., Bozorgmehry B.R., Kazemeini M., CFD Modeling of Gas-Liquid Hydrodynamics in a Stirred Tank Reactor, *Iran. J. Chem. Chem. Eng. (IJCCE)*, **26**(2): 85-96 (2007).

[34] Ottino J.M., "The Kinematics of Mixing: Stretching, Chaos, and Transport", Cambridge University press, Cambridge (1989).